Journal of Industrial and Engineering Chemistry 101 (2021) 135–143

Contents lists available at ScienceDirect

Journal of Industrial and Engineering Chemistry

journal homepage: www.elsevier.com/locate/jiec

Design and synthesis of the quinacridone-based donor polymers for application to organic solar cells

Doo Hun Kim, Sung Jae Jeon, Yong Woon Han, Young Hoon Kim, Nam Gyu Yang, Hyoung Seok Lee, Doo Kyung Moon *

Nano and Information Materials (NIMs) Laboratory, Department of Chemical Engineering, Konkuk University, 120 Neungdong-ro, Gwangjin-gu, Seoul 05029, Republic of Korea

ARTICLE INFO

Article history:
Received 31 May 2021
Revised 17 June 2021
Accepted 20 June 2021
Available online 25 June 2021

Keywords:
Organic solar cells
Quinacridone
Benzothiadiazole
Quinoxaline
π-Spacer
Thienothiophene

ABSTRACT

D–π–A type quinacridone-based polymers were designed with different acceptor moieties and successfully synthesized via a Suzuki coupling reaction. Depending on the introduction of benzothiadiazole and quinoxaline moieties, the synthesized polymers, poly(quinacridone-thienothiphene-benzothiadiazole) (PQCfTB) and poly(quinacridone-thienothiphene-quinoxaline) (PQCfTQx), showed different physical, optical and electrochemical properties. PQCfTB had a more extended π-conjugation length and a higher number average molecular weight (M_n, 365.1 kDa) than that of PQCfTQx (167.5 kDa). Furthermore, each polymer showed different optical behavior and optical band gaps (E_g^{opt}: 1.91 eV for PQCfTB; 1.87 eV for PQCfTQx) in the film state. The highest occupied molecular orbital (HOMO) and lowest unoccupied molecular orbital (LUMO) levels of PQCfTB and PQCfTQx were calculated as −5.20 eV and −5.22 eV, as well as −3.29 eV and −3.35 eV, respectively. The XRD measurement results showed that the polymers for PQCfTB and PQCfTQx had bimodal and face-on structures, respectively. Finally, organic solar cells for both polymers were fabricated and optimized with respect to the acceptor. In summary, the PQCfTB-based devices showed higher power conversion efficiencies (w/$PC_{71}BM$ 3.9%; w/IT-M 5.2%; w/PM6:Y6-BO-4Cl 11.0%) than PQcfTQx (2.3%, 4.7%, and 10.0%).

Introduction

With recent developments in molecular engineering, π-conjugated polymers as organic semiconductors have attracted much attention in the research field of electronic devices [1–6]. π-Conjugated polymer-based organic solar cells (OSCs) have several advantages; they can be manufactured through a simple solution process and are low-cost, lightweight, highly flexible, and ideal for mass production via roll-to-roll processing [7–14]. Bulk heterojunction (BHJ) system, which are blend types of electron donors and acceptors, have been employed in the preparation of the active layer coating in OSCs [15–18]. Recent studies on BHJ systems have focused on non-fullerene acceptors (NFAs) [19–25]. With the recent development of NFAs, the power conversion efficiency (PCE) of single-junction OSCs based on NFAs has reached over 18% [26–28].

π-Conjugated polymers as electron donors are donor–acceptor (D–A)-type or donor–spacer–acceptor (D–π–A) type copolymers in which the electron-donating unit (D) and electron-accepting unit (A) are bonded alternately. In the molecular structure designs of π-conjugated polymers, the energy level can be effectively controlled by the selection of suitable D and A building blocks or π-spacers [28–31]. The incorporation of these has been reported to have significantly influence the high open-circuit voltage (V_{OC}), short-circuit current density (J_{SC}), and fill factor (FF) to achieve a high PCE of BHJ OSCs [32,33].

The introduction of π-spacers to enhance the properties of D–π–A type conjugated copolymers has recently gained attention. The introduction of π-spacers yields the following results: (1) changes in optical and electrochemical properties owing to an increase in conjugation length in D–A copolymers, (2) improved charge transfer properties owing to increased planarity, and (3) close packing of polymers by improving intermolecular π–π interactions owing to steric hindrance [34].

Thieno[3,2-b]thiophene (TT) is a well-known π-spacer of a highly efficient D–A copolymer owing to coplanar fused aromatic rings and large molecular planes [35]. TT can enhance the backbone planarity of the copolymer as well as the delocalization of π-electrons. TT increases the HOMO level of the polymers; thus

* Corresponding author.
E-mail address: dkmoon@konkuk.ac.kr (D.K. Moon).

https://doi.org/10.1016/j.jiec.2021.06.020
1226-086X/

in turn increases the optical absorption area and further improves the charge carrier mobility, resulting in an increase in the *Jsc* value of the OSC. Hou et al. compared and analyzed the optical and, electrochemical properties and crystallinity of polymers depending on thiophene (T) and thienothiophene (TT). In particular, the study found that TT has a significant influence on the intermolecular interactions of conjugated polymers, which induces morphological changes in film formation [36]. Wang et al. introduced T and TT to benzothiadiazole (BT) for polymer design. Consequently, BDT-TT-BT (11.34 mA/cm^2) polymers with TT spacer showed a higher *Jsc* value than BDT-T-BT (9.45 mA/cm^2) with the introduction of the T spacer, thereby increasing the PCE [37]. Furthermore, the TT spacer plays a role in lowering the tilting angle between D and A. This reduction strengthens intermolecular π–π orbital stacking, which in turn induces well-ordered laminar packing.

Our group has synthesized D–π–A type polymers in which T spacer was introduced into the D–A structure having quinacridone (QC)–BT and QC–quinoxaline (Qx) as main backbone, respectively. T spacer induced the change in the twist angles between donor and acceptor, and further influences the planarity and crystallinity. As a result, both polymers based on QC–T–BT (named as PQCDTB) and QC–T–Qx(named as PQCDTQ) exhibited edge-on and face-on ordered properties, respectively [38].

QC derivatives, which are known as red-violet pigments, have been attracting attention as organic thin film transistors (OTFTs) materials owing to their high crystallinity and self-assembly characteristics, as well as high mobility [39,40]. Moreover, weak donor QCs were confirmed to decrease the charge transfer in D–A type polymers because an extreme increase in the π-bridge weakens the electron-donating property of the donor unit [30]. Qx derivatives can be structurally varied to exhibit high solubility and electronic properties through various substituents [31]. BT derivatives have been widely used as acceptors because of their strong electron affinity from the coplanar symmetric structure [41].

Based on these basic theories, in this study, we synthesized two polymers, "poly(quinacridone-thienothiphene-benzothiadiazole) (PQCfTB)" and "poly(quinacridone-thienothiphene-quinoxaline) (PQCfTQx)," in which the QC derivative and TT were used as the donor and π-bridge of the D–π–A copolymer, respectively, and Qx and BT were introduced as acceptors. The physical, optical, and electrochemical properties of both polymers were systematically investigated, and they were subsequently used to fabricate efficient OSCs.

Experimental section

Materials

All the reagents were purchased from Aldrich and used without further purification. The final monomers (M1, M2, and M3) were synthesized and prepared according to our previous reports [30,42,43].

Polymerization

Poly[quinacridone-thienothiophene-benzothiadiazole] (PQCfTB)

M1 (0.27 g, 0.25 mmol), M2 (0.20 g, 0.25 mmol), and Pd $(PPh_3)_4$(0) (0.009 g, 0.008 mmol) and Aliquat 336 were added in a Schlenk tube three vacuum/nitrogen purging cycles were performed. Under a nitrogen atmosphere, 2 M degassed aqueous K_2CO_3 (10 mL) and anhydrous toluene (25 mL) were poured into a reactor. The mixture was heated to 90–95 °C and stirred for 24 h in the dark. To complete the polymerization, the polymer was end-capped with 2-bromothiophene (2–3 drops). After cooling the reactor to the room temperature, the mixture was poured into methanol. The precipitate was filtered off through a thimble and purified by Soxhlet extraction using the different solvents in the following order: methanol (24 h), acetone (12 h), hexane (24 h), and chloroform (24 h). The polymer was recovered from the chloroform fraction and re-precipitated in methanol. After filtration through a Buchner funnel, the final product was obtained after drying under vacuum. (Dark-purple solid, 0.27 g, 67%) ^{1}H NMR (400 MHz, $CDCl_3$) δ(ppm): Supporting Information, Fig. S1. Anal. Calcd for $C_{94}H_{130}N_4O_4S_5$: C, 73.29; H, 8.51; N, 3.64; O, 4.15; S, 10.41;. Found: C, 71.51; H, 9.15; N, 3.62; O, 5.12; S, 10.28;

Poly[quinacridone-thienothiophene-quinoxaline] (PQCfTQx)

PQCfTQx was synthesized using the same procedure as that used for PQCfTB by using M3 instead of M2 (Red solid, 0.25 g, 59%). ^{1}H NMR (400 MHz, $CDCl_3$) δ(ppm): Supporting Information, Figure S2. Anal. Calcd for $C_{106}H_{140}N_4O_4S_4$: C, 76.91; H, 8.37; N, 3.32; O, 3.79; S, 7.60. Found: C, 76.74; H, 8.42; N, 3.30; O, 3.82 S, 7.51.

Results and discussion

Scheme 1 shows the chemical structures of the polymerization process using each monomer. As shown in Scheme 1, quinacridone (M1), benzothiadiazole (M2), and quinoxaline (M3) were used as monomers to synthesize two polymers, PQCfTB and PQCfTQx, through the Suzuki coupling reaction. The yields of the obtained polymers, which were a dark-purple and red solid, were 67 % and 59 %, respectively. These polymers are well soluble in typical solvents such as chloroform, chlorobenzene (CB), and *o*-dichlorobenzene (ODCB). The structures of the synthesized polymers were identified by nuclear magnetic resonance (NMR) and elemental analysis (EA).

Table 1 lists the molecular weights and thermal properties of PQCfTB and PQCfTQx. As shown in Table 1, according to the standard gel permeation chromatography (GPC) measurement results on polystyrene, the number average molecular weights (M_n) of PQCfTB and PQCfTQx were 365.1 kDa and 167.5 kDa, respectively, while their polydispersity indices (PDI = M_w/M_n) were calculated as 3.13 and 2.13, respectively. Their molecular weights were 4 to 8 times that of synthetic polymers with T introduced as spacers [38]. These observations can be explained by the molecular structural changes caused by the intermolecular steric hindrance between the donor and acceptor molecules depending on the spacer.

As shown in Table 1, PQCfTB and PQCfTQx exhibited thermal stabilities of 300 °C or higher which are required for OSCs or other applications in opto-electronic devices. Additionally, the increase in molecular weight indicates that the polymers can absorb more photons owing to the conjugation expansion; thus, possibly providing a high photon current.

Optical and electrochemical properties

Fig. 1 shows the normalized UV–vis spectra of D–π–A polymers (PQCfTB and PQCfTQx) with TT introduced as spacer in chloroform solution state (10^{-6} M) and the as-cast thin film state; the results are summarized in Table 2. The latter measurements were obtained using a film with a thickness of 50 nm formed by spin-coating.

The absorption peaks (λ_{max}) of both polymers were observed at 350–450 nm, which correspond to the UV–vis spectra owing to the $\pi - \pi^*$ transition of the conjugated backbone in solution and film states. In addition, other λ_{max}s of both polymers were observed at 450–650 nm, which occurred owing to intramolecular charge transfer (ICT) between the donor and acceptor moieties [44]. The

Results and Discussion

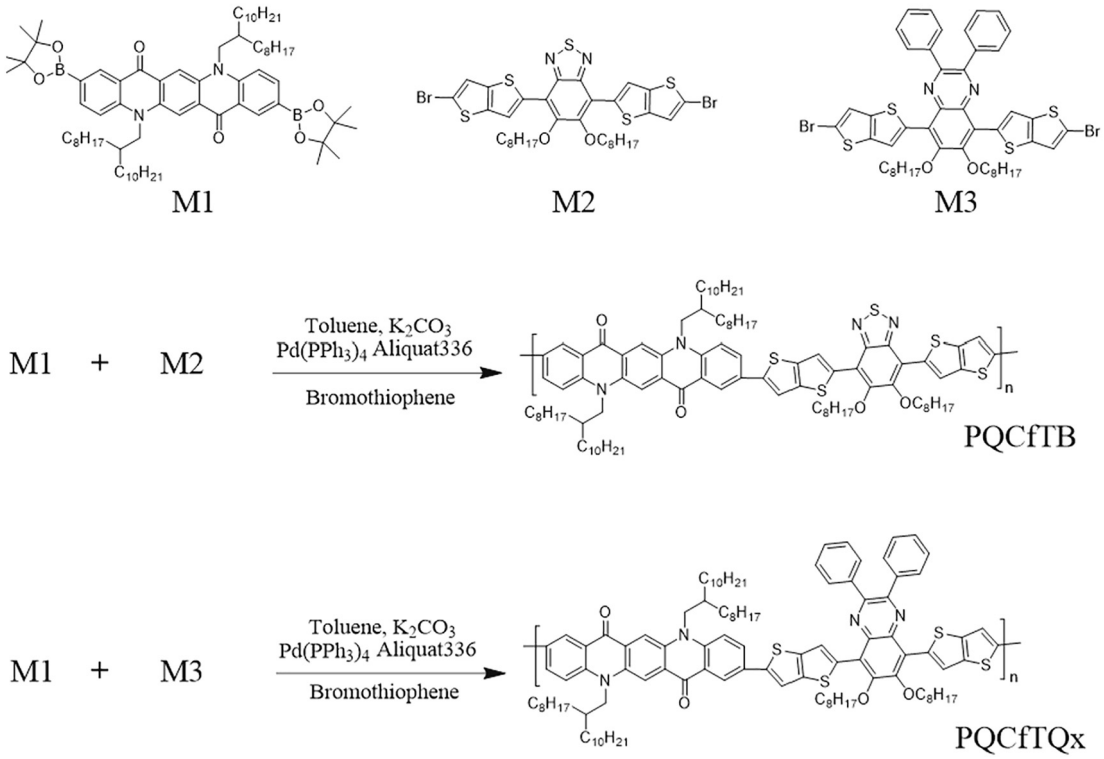

Scheme 1. Scheme of the polymerization for PQCfTB and PQCfTQx.

Table 1
Molecular weight and thermal properties of the polymers.

Polymer	Yield [%]	M_n (kDa)	M_w (kDa)	PDI	Degree of polymerization	T_d (°C) [a]
PQCfTB	67	365.1	1145.7	3.13	237	328
PQCfTQx	59	167.5	357.0	2.13	99	332

[a] Temperature resulting in 5% weight loss based on initial weight.

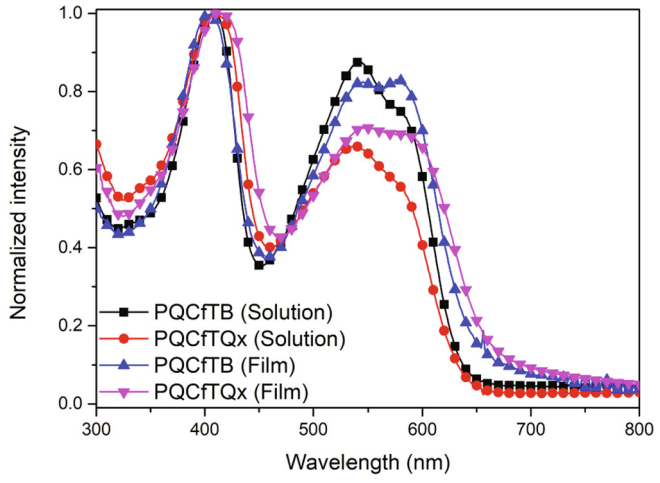

Fig. 1. Normalized absorption spectra of polymers in solution and film states.

ICT peaks were red-shifted by ~10 nm in the film state compared to the solution phase and the intensity of the shoulder peaks slightly increased. These shoulder peaks show similar absorption areas regardless of the acceptor structure. The formation of a red-shift and shoulder peak suggests strong intermolecular interactions in polymers according to the planar backbone structure in the film state. This observation is consistent with the previous result that the TT spacer enhanced the planarity between the donor and acceptor, and further effectively increased the conjugation of the polymer main chain [30]. Furthermore, when we introduced TT as a π-bridge, we observed that the shape of the molecular chains changed from a z-shaped to a straight-line because of the increase in the absorption area and conformation lock in comparison to T [30,37]. In particular, strong shoulder peaks were observed in the solution phase of two polymers (PQCfTB and PQCfTQx) as in the thin film, which confirmed that aggregation or orderly π–π stacking between polymer chains is present in dilute solution [43]. This observation is consistent with the study by Hou et al., who reported that D–π–A type polymers with TT introduced as a spacer showed J-aggregate phenomenon in the film and solution phases [36].

The film band edges of PQCfTB and PQCfTQx were calculated as 649 nm and 663 nm, respectively, which indicates the absorption of the wavelength over a wide range, and the optical band gap energies were calculated as 1.91 eV and 1.87 eV, respectively. These results show that TT changes the planar structure of the polymers and widens their absorption area to reduce the band gap.

Fig. 2 shows the cyclic voltammetry (CV) measurements of the polymers. CV measurement was taken to identify the HOMO and

Table 2
Optical and electrochemical data of polymers.

Polymer	UV–vis absorption					$E_g^{opt,a}$[eV]	Cyclic voltammetry		
	$CHCl_3$ solution		Film				E_{ox}^{onset}[V]	HOMO[b][eV]	LUMO[b][eV]
	λ_{max} [nm]	λ_{sh} [nm]	λ_{max} [nm]	λ_{sh} [nm]	λ_{onset} [nm]				
PQCfTB	407, 541	583	407, 545	583	649	1.91	0.84	−5.20	−3.29
PQCfTQx	408, 536	584	413, 549	585	663	1.87	0.86	−5.22	−3.35

[a] Calculated from the intersection of the tangent on the low-energy edge of the absorption spectrum with the baseline.
[b] $E_{HOMO\ (or\ LUMO)} = -[E_{onset}(\text{vs. Ag/AgCl}) - E_{1/2}(Fc/Fc^{+}\ \text{vs. Ag/AgCl})] - 4.8$ eV.

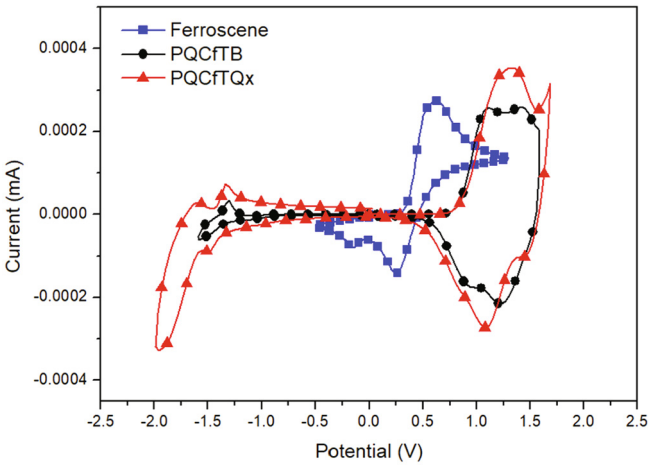

Fig. 2. Cyclic voltammogram of polymers.

LUMO levels of PQCfTB and PQCfTQx polymers, and the results are shown in Table 2 and Fig. 2. The oxidation onset potential of PQCfTB and PQCfTQx was 0.84 V and 0.86 V, respectively, while their corresponding HOMO levels were calculated to be −5.20 eV and −5.22 eV, respectively. The LUMO energy level was derived by calculating the differences in the HOMO levels and optical band gap energy. Thus, the LUMO levels of PQCfTB and PQCfTQx were −3.29 eV and −3.35 eV, respectively. The HOMO levels of PQCfTB and PQCfTQx were slightly higher owing to the strong donating characteristics of the TT unit [41].

DFT calculation

For a better understanding of the electric properties of the synthesized polymers, as well as the molecular geometries and electron density of states distribution, simulations were performed using density functional theory (DFT). Fig. 3 and Table 3 show the calculated HOMO and LUMO orbitals and dihedral angles. As shown in Fig. 3, in the LUMO orbitals of PQCfTB and PQCfTQx, electrons are localized in the acceptor unit, including the spacer, because of the electron-deficient character of the acceptor unit owing to the presence of two imine nitrogens and quinoid structures, which have electron-withdrawing properties. Moreover, in the HOMO orbitals, electrons are delocalized widely through the polymer main chain, including quinacridone, the spacer, and the acceptor. This phenomenon suggests that charge transfer occurs smoothly from donor to acceptor when the energy levels of PQCfTB and PQCfTQx are transmitted from the HOMO to the LUMO [30].

In addition, this result is consistent with a previous report which revealed that the introduction of TT as a π-bridge unit can help form a straight conformation (L-type) capable of controlling the conformation of the polymer backbone [36]. According to the DFT calculation results shown in Table 3, the HOMO levels of PQCfTB and PQCfTQx were −4.7 eV and −4.8 eV, respectively, and their LUMO levels were −2.3 eV and −2.5 eV, respectively. The HOMO and LUMO of PQCfTB are higher than those of PQCfTQx because BT possesses higher electron-withdrawing characteristics than Qx. These results show a similar tendency to the CV measurement results shown in Table 2.

As shown in Fig. 3 and Table 3, the TT spacer was twisted in the front direction in PQCfTB and the back direction in PQCfTQx. Furthermore, the S atom of TT engages in attractive Coulomb interactions with the N and O atoms of BT and Qx in the two polymers. Thus, conformational locks formed in the two polymers, showing a small dihedral angle (−21.2° to 23.5°) [45]. The dihedral angles of PQCfTB were 23.1°, 15.2°, 15.5°, and 23.5°, confirming twists occur in the same direction. Thus, the growth structure of the polymers showed a helical geometry. Petter Persson reported that polymers with a helical geometry formed intramolecular ordering that facilitated extensive electronic conjugation and further showed more active electron migration within polymers [46]. The dihedral angles of PQCfTQx were −21.2°, 12.8°, 12.0°, and 0.4°, indicating a planar polymer backbone because the polymers did not revolve owing to the offset in values between the twisting part in the back direction (θ_1) and the revolving part in the front direction (θ_2, θ_3). Thus, the polymers have enhanced crystallinity and ordered orientation as the steric hindrance between the main chains of the polymers is reduced and the intermolecular interaction between the polymer chains is increased.

Crystallinity analysis

X-ray diffraction (XRD) was performed to analyze the structural order in the polymers, and the results are shown in Fig. 4. The results were summarized in Table 4. In the diffraction patterns of out-of-plane mode for PQCfTB and PQCfTQx, both polymers showed strong lamellar peaks at near 4.52° and 4.30°, respectively. According to the calculation from Bragg's law ($\lambda = 2d\sin\theta$), PQCfTB has a closer *d*-spacing (19.55 Å) than that of PQCfTQx (20.55 Å), which arises from the difference of aggregation ability for polymer curvatures. More specifically, PQCfTB having twist backbone showed the long-range order with intense (200) and (300) diffractions, which exhibited high crystallinity of inherent nature. In addition, a broad diffraction peak appeared at around 24°, which represented a crystal plane associated with π–π stacking (010), where the π-π stacking distance ($d_{(010)}$) of PQCfTB and PQCfTQx was calculated as 3.63 and 3.74 Å, respectively. These values were smaller than the $d_{(010)}$ value (4.0–4.4 Å) of the benzene-thiophene linkage reported in other articles [47].

In the diffraction pattern of PQCfTB in the in-plane mode, bimodal structure was found with peaks appearing near the (010) crystal plane. On the other hand, any peaks of PQCfTQx did not appear near 24–25°, which is attributed to strong π–π stacking properties of polymer [44,48,49]. In general, π–π stacking of polymer chains allows the charges between the chains to be delocalized, and as a result, face-on structure helps to charge transport in the vertical direction. However, a bimodal structure comprising a mixture of face-on and edge-on packing can lower the charge transport bar-

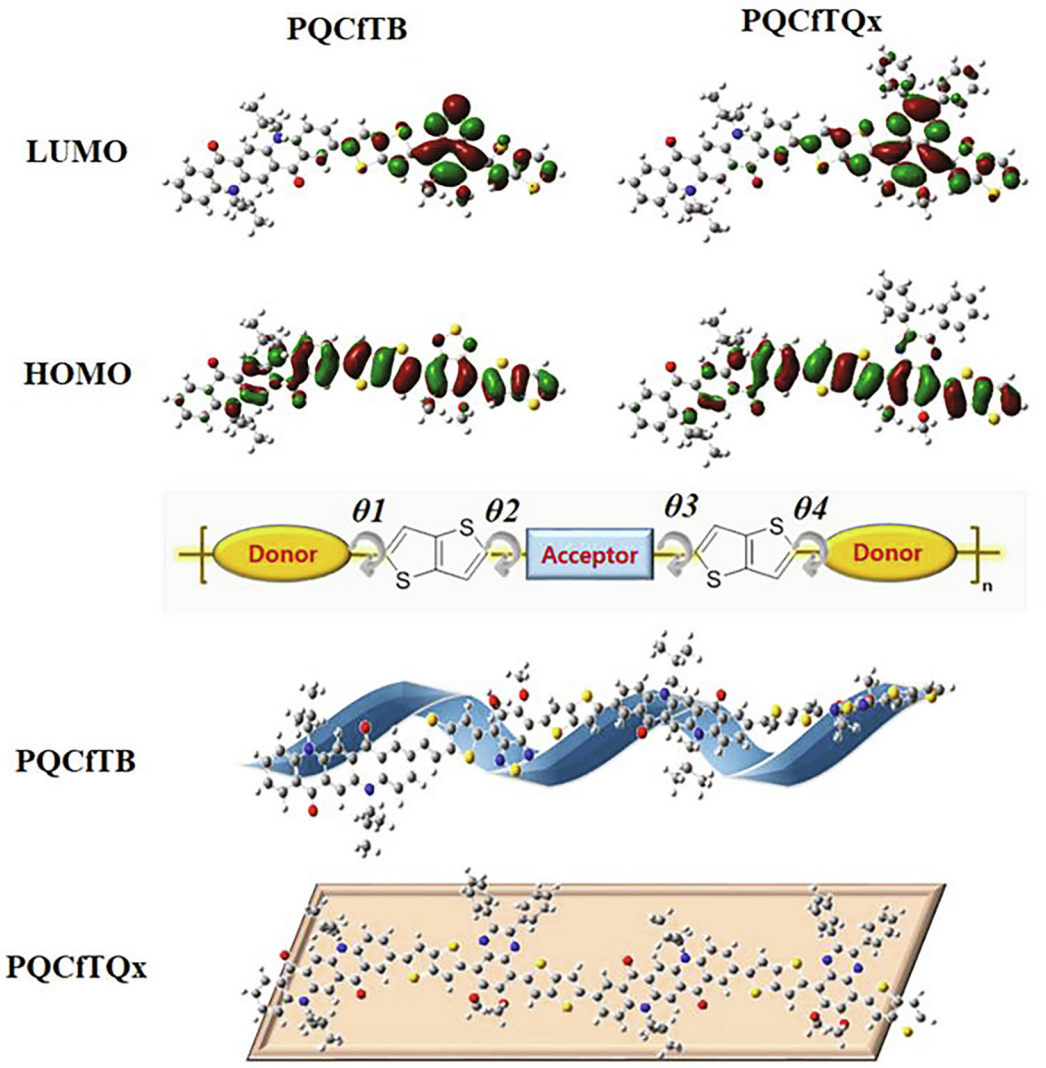

Fig. 3. Calculated LUMO and HOMO orbitals and dihedral angles of the dimer model compounds for PQCfTB and PQCfTQx.

Table 3
Calculated DFT data of the dimer model compounds for PQCfTB and PQCfTQx.

Polymer	$HOMO^{cal.}$ [eV]	$LUMO^{cal.}$ [eV]	Dihedral angle (degree)			
			θ_1	θ_2	θ_3	θ_4
PQCfTB	−4.7	−2.3	23.1	15.2	15.5	23.5
PQCfTQx	−4.8	−2.5	−21.2	12.8	12.0	0.4

rier between domains and can be advantageous for three-dimensional charge collection in BHJ OSCs. Further, it can contribute to efficient charge generation as the domain size decreases [50].

Photovoltaic performance

We fabricated conventional BHJ OSCs to investigate the photovoltaic (PV) properties of the synthesized polymers with respect to the acceptor. The PV properties of both polymers were assessed using OSC devices with ITO/PEDOT:PSS/PV materials/PDINN/Ag structure. Each polymer was optimized by changing the weight ratio of the acceptors and solvent conditions. The details have been provided in the Supporting Information and Fig. 5.

Fig. 6 shows the *J*–*V* curves of each polymer upon varying the acceptor, while Fig. 7 shows the EQE spectra under the same conditions. *J*–*V* characteristics were measured under ambient atmosphere, and the active area was 4 mm^2. Table 5 summarizes of the PV properties of the fabricated OSCs.

As shown in Table 5, the PQCfTB-based device showed PCE of 3.9% based on V_{OC}, J_{SC}, and FF of 0.74 V, 9.21 mA/cm^2, and 57.02%, respectively. The values for J_{SC} and FF were higher than those of the PQCfTQx:$PC_{71}BM$-device, and thus, PCE was improved. It is also believed that the introduction of BT resulted in increased molecular weight and expanded light absorption range at long wavelengths. Compared with PQCfTB:$PC_{71}BM$, PQCfTQx:$PC_{71}BM$-device showed poor J_{SC}, in particular. This may be owing to the strong π–π stacking properties of PQCfTQx, which did not allow smooth blending with $PC_{71}BM$, i.e., the electron acceptor. When

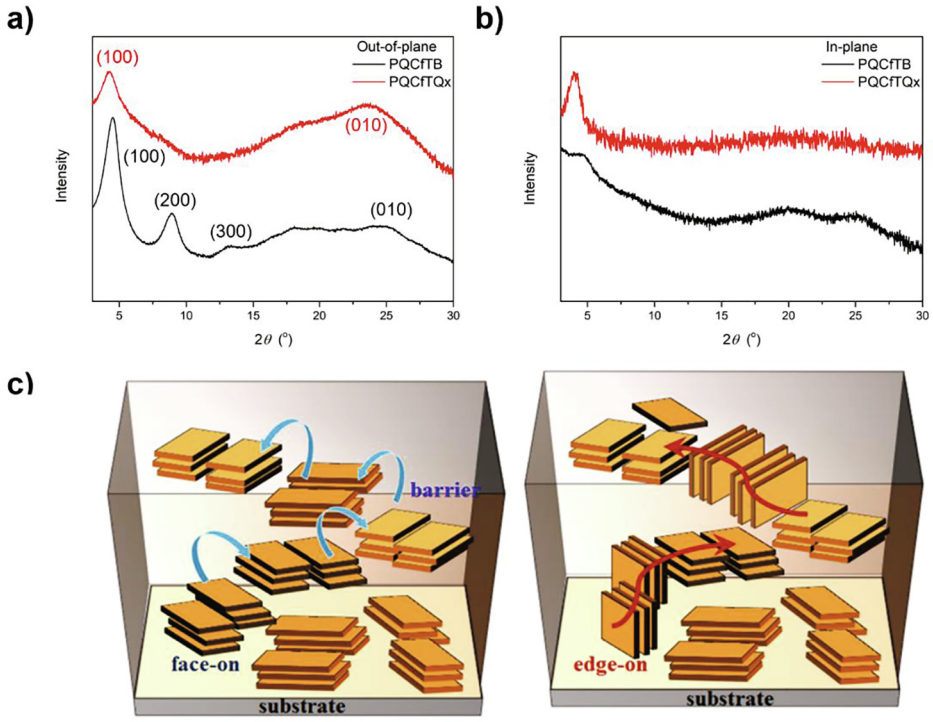

Fig. 4. (a) Out-of-plane and (b) in-plane X-ray diffraction patterns of thin films for each polymer. (c) Schematic representation of interdigitated packing structure.

Table 4
XRD results of thin films for each polymer in out-of-plane.

Polymer	$d_{(100)}$ [Å] at 2θ [°]	$d_{(200)}$ [Å] at 2θ [°]	$d_{(300)}$ [Å] at 2θ [°]	$d_{(010)}$ [Å] at 2θ [°]
PQCfTB	19.55 at 4.52	9.89 at 8.94	6.63 at 13.36	3.63 at 24.54
PQCfTQx	20.55 at 4.30	–	–	3.74 at 23.80

IT-M was blended with each polymer, both devices for PQCfTB:IT-M and PQCfTQx:IT-M showed a slightly improved performance with PCE up to 5.2% and 4.8%, respectively, compared to the fullerene-based devices. The V_{OC} and J_{SC}s of IT-M-based devices are significantly higher than those of $PC_{71}BM$-based devices. This is because of the energy loss and light absorption range difference between the acceptor materials. The details are described in the part of charge transfer analysis.

To test the accuracy of the device measurements, the external quantum efficiency (EQE) was measured, and EQE curves based on the maximum efficiency of each polymer were drawn. Because the EQE curves are created in the polymer phase where most photons are generated, they are correlated with the absorption range of the polymer [51]. As shown in Fig. 7, the calculated J_{SC}s of all the fabricated devices were determined from the *J–V* curves within a 5% mismatch. Specifically, most of the $PC_{71}BM$-based devices

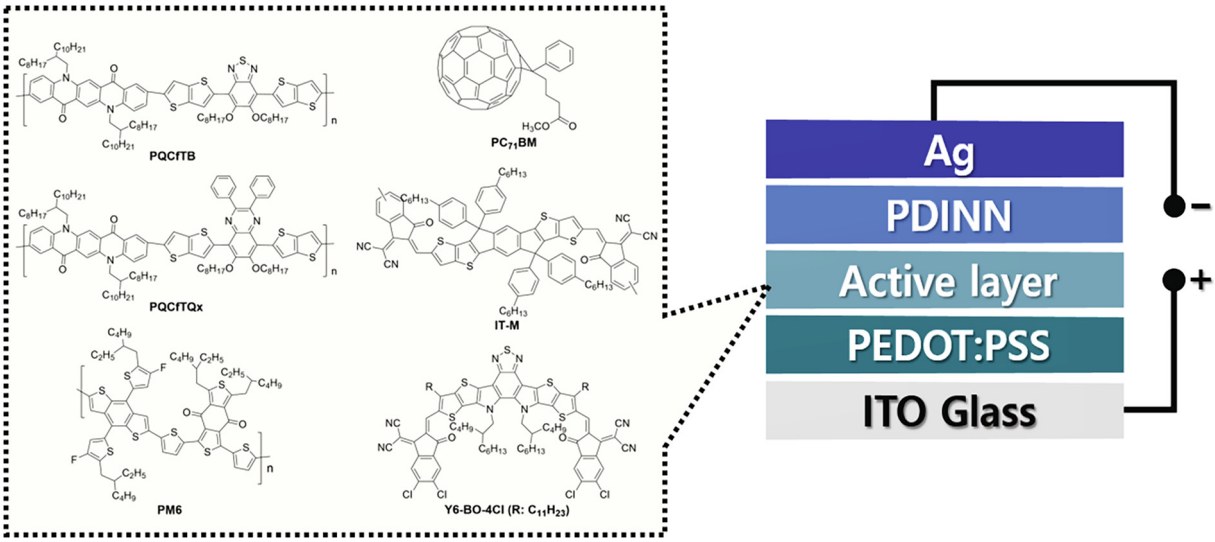

Fig. 5. Photovoltaic materials (PQCfTB, PQCfTQx, and PM6 as donor, respectively; $PC_{71}BM$, IT-M, and Y6-BO-4Cl as acceptor, respectively) and device structure of the OSCs.

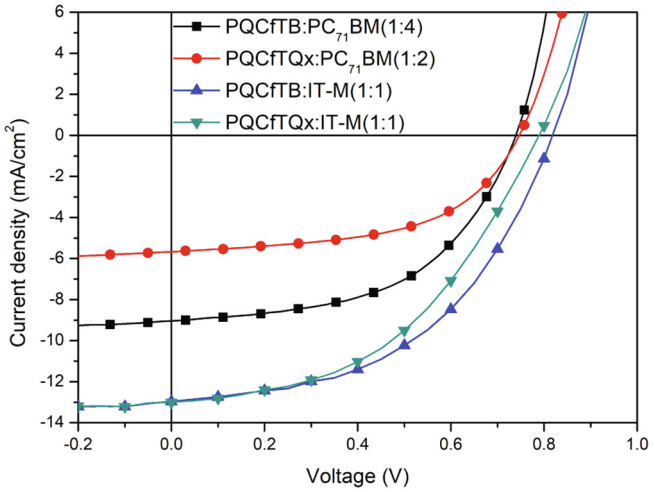

Fig. 6. *J-V* curves of the OSCs based on the polymers with respect to the acceptor.

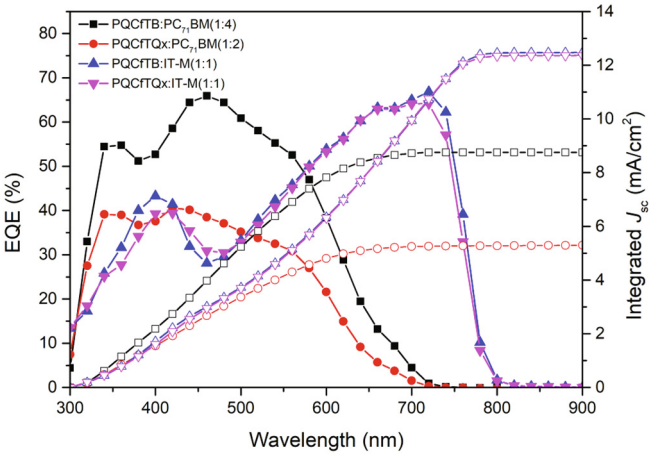

Fig. 7. EQE curves with integrated Jsc of the OSCs based on the polymers with respect to the acceptor.

showed EQE responses in the range of 300–700 nm according to the absorption range of the polymer. The IT-M-based devices, having a low band gap acceptor, had extended EQE curves in the range of 300–800 nm, which is consistent with the tendency of J_{SC} [52,53].

To further examine the effect in the ternary blend, a high-efficiency active combination, PM6:Y6-BO-4Cl was used to fabricate the devices. As shown in Fig. S3, both polymers of PQCfTB and PQCfTQx have complementary optical and electrochemical properties to those of PM6:Y6-BO-4Cl. The binary blend-based device of PM6:Y6-BO-4Cl showed a reasonable PCE of 14.4% with V_{OC} of 0.847 V, J_{SC} of 25.7 mA/cm^2, and FF of 66.0% in comparison with the literature [54]. However, the ternary blends of PQCfTB and PQCfTQx showed relatively poor performances with PCEs of 11.0% and 10.0%, respectively, because the polymers acted as traps, such as charge recombination in each device. This might be caused by the polymers having low compatibility with materials, and especially, large differences in frontier energy levels with Y6-BO-4Cl. The details of the PV results are displayed and summarized in the Supporting Information (Fig. S4 and 5 and Table S1).

Morphology analysis

The surface morphology of the polymer blend is an important determining factor for OSC efficiency [55]. Among the results of OSC devices for each polymer, the morphologies of fullerene-based blend films that showed large differences in PCE were examined via atomic force microscopy (AFM), the results of which are shown in Fig. 8. As shown in Fig. 8a, PQCfTB:$PC_{71}BM$ showed a fibril-like surface, which is beneficial to phase separation. With respect to the nanoscale features, a root-mean-square (RMS) roughness of 2.3 nm was found. Contact between the long polymer backbones was used to form a charge transport pathway within the ordered zone, which facilitated the movement of the charge carriers. This result is consistent with the J_{SC} value of PQCfTB.

Conversely, as shown in Fig. 8b, PQCfTQx:$PC_{71}BM$ showed RMS roughness of 1.8 nm by forming island-type domain and macrophase-type of domain owing to strong aggregation of PQCfTQx. Similar results also appeared in the phase images, where the PQCfTB:$PC_{71}BM$ film was smooth; however, PQCfTQx:$PC_{71}BM$ showed an aggregated film. This interferes with the effective separation of excitons and produces a low J_{SC} [56–58]. This was confirmed by the same results for J_{SC} and IPCE shown in Table 5.

Charge transfer analysis

To investigate the influence of each active layer on exciton dissociation and charge transfer in the optimized devices, photoluminescence (PL) measurements of pristine and blend films are performed and the relevant spectra are presented in Figs. S6 and S7. At the used excitation wavelength of 530 nm and 630 nm, respectively, the PL spectra of the active layers are located in the range of 550–900 nm. The details are summarized in Table S2. In short, as introducing the acceptor from fullerene ($PC_{71}BM$) to non-fullerene (IT-M), each polymer blend film showed the increased PL quenching (PLQ) rates, which is attributed to decrease energy offsets between materials according to enhanced energy level alignments (Table S3 and Fig. S8). On the other hand, the PM6:Y6-BO-4Cl-based ternary blend of each polymer showed the poor PLQ rates compared with binary blend of PM6:Y6-BO-4Cl. This result may be caused by large gap of HOMO and LUMO energy offsets between materials.

Table 5
Photovoltaic performance of the BHJ solar cells.

D:A ratios	V_{OC} (V)	J_{SC} (mA/cm^2)	Calculated J_{SC} (mA/cm^2)	FF (%)	PCE (%)
PQCfTB:$PC_{71}BM$ = 1:4	0.74 (0.73 ± 0.01)	9.21 (9.10 ± 0.11)	8.75	57.02 (56.52 ± 0.50)	3.9 (3.75 ± 0.15)
PQCfTQx:$PC_{71}BM$ = 1:2	0.74 (0.73 ± 0.01)	5.70 (5.60 ± 0.10)	5.29	55.00 (54.56 ± 0.44)	2.3 (2.20 ± 0.10)
PQCfTB:IT-M = 1:1	0.82 (0.80 ± 0.02)	12.97 (12.75 ± 0.22)	12.42	49.16 (49.01 ± 0.15)	5.2 (5.10 ± 0.12)
PQCfTQx:IT-M = 1:1	0.79 (0.79 ± 0.00)	12.95 (12.64 ± 0.31)	12.33	46.29 (46.1 ± 0.19)	4.8 (4.5 ± 0.25)

The average and standard deviations of multiple devices (4–10) are shown in brackets.

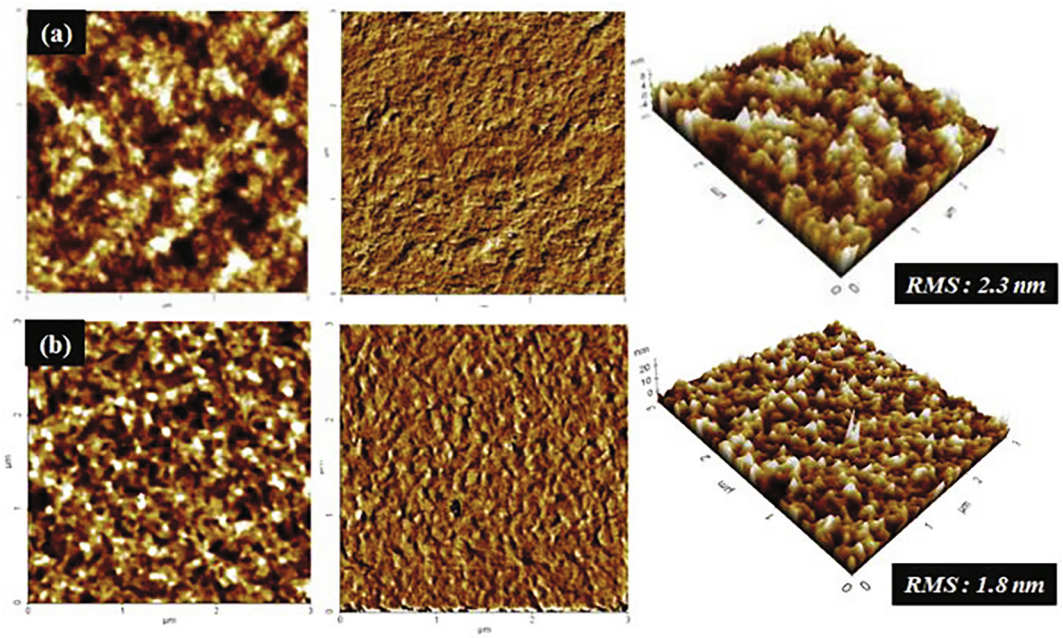

Fig. 8. Topographic AFM images of (a) PQCfTB:$PC_{71}BM$ = 1:4 (b) PQCfTQx:$PC_{71}BM$ = 1:2. The imaging size is 3 × 3 μm^2 for each panel: 2D and 3D height images (left and right) and 2D phase images (center).

Successively, we further studied the energy loss from the optical band gaps (E_g^{opt}) from the EQE spectra for each optimized device by using the formula ($E_{loss} = E_g^{opt} - eV_{OC}$; e is elementary charge). The calculated energy loss (E_{loss}) values are summarized in Table S42. In summary, the E_{loss}s of both polymers were sequentially decreased by blending with $PC_{71}BM$, IT-M, and PM6:Y6-BO-4Cl, respectively. Although the decreased the efficiency in comparison of binary blend, both ternary devices based on suppressed E_{loss}s showed the PCEs over 10% with decent V_{OC} of 0.80–0.81 V.

For providing insight of carrier recombination characteristics, light intensity dependence of J_{SC} and V_{OC}, dark current density–voltage properties were analyzed as shown in Figs. S9–S11 [59–62]. For illumination intensity (I), the equations of $J_{SC} \propto I^{\alpha}$ and $V_{OC} \propto kT/q\ln(I)$ exhibits suppressed carrier recombination with slope values approaching 1.0 (where, k is Boltzmann constant, T is the absolute temperature, and q is the elementary charge). In Figs. S9 and S10, PQCfTB showed slope values close to 1.0 in devices with either $PC_{71}BM$ or IT-M (α = 0.998, 0.995 and slope = 1.10 kT/q, 1.121 kT/q) while PQCfTQx showed those relatively not close to 1.0. Also, in Fig. S11, PQCfTB showed lower leakage current in reverse bias and higher current density in range over 0.74 V. These reflected that PQCfTB exhibited high shunt resistance (R_{Sh}) of 282.1 and 609.6 Ω cm^2 in order of $PC_{71}BM$ and IT-M with low leakage current, while those of PQCfTOx were low (246.0 and 472.4 Ω cm^2). These results provided efficient carrier dissociation and suppressed carrier recombination properties, which are consistent with the electron and hole mobility characteristics in Table S5.

Conclusions

In this study, two D–π–A type PQCfTB and PQCfTQx were sucessfully synthesized through a Suzuki coupling reaction using a donor (quinacridone), acceptor (benzothiadiazole, quinoxaline), and π-spacer (thienothiphene). The introduction of TT reduced the steric hindrance, thereby showing a high molecular weight and good thermal stability. The optical band gap, HOMO, and LUMO values of PQCfTB and PQCfTQx were calculated as 1.91 eV, −5.20 eV, and −3.29 eV as well as 1.87 eV, −5.22 eV, and −3.35 eV, respectively. Two types of λ_{max} peaks in the film states for both polymers were observed in the corresponding UV–vis spectra. Furthermore, a wide optional absorption area, ranging from 350 nm to 700 nm, was observed, owing to π − π* transition of conjugated backbone as well as ICT effect. In particular, the devices fabricated using PQCfTB with a high molecular weight and bimodal structure blended with each acceptor showed higher PCE's than the corresponding devices fabricated using PQCfTQx. The changes in the shape of the polymer backbone and the ordered characteristics within the film were identified in this study, enabling us to derive the design and engineering considerations of conjugated polymer-based OSCs.

Declaration of Competing Interest

The authors declare that they have no known competing financial interests or personal relationships that could have appeared to influence the work reported in this paper.

Acknowledgment

This paper was supported by Konkuk University in 2017.

Appendix A. Supplementary data

Supplementary data to this article can be found online at https://doi.org/10.1016/j.jiec.2021.06.020.

References

[1] R.H. Friend, R.W. Gymer, A.B. Holmes, J.H. Burroughes, R.N. Marks, C. Taliani, D. D.C. Bradley, D.A. Dos Santos, J.L. Brédas, M. Lögdlund, W.R. Salaneck, Nature 397 (1999) 121.
[2] T. Yamamoto, H. Kokubo, M. Kobashi, Y. Sakai, Chem. Mater. 16 (2004) 4616.
[3] S. Grigorian, D. Tranchida, D. Ksenzov, F. Schäfers, H. Schönherr, U. Pietsch, Eur. Polym. J. 47 (2011) 2189.
[4] S. Samson, J. Rech, L. Perdigón-Toro, Z. Peng, S. Shoaee, H. Ade, D. Neher, M. Stolterfoht, W. You, ACS Appl. Polym. Mater. 2 (2020) 5300.
[5] C. Duan, L. Ding, Sci. Bull. 65 (2020) 1422.

[6] Q. Lv, C. An, T. Zhang, P. Zhou, J. Hou, Polymer (Guildf). 218 (2021).
[7] A.J. Heeger, Adv. Mater. 26 (2014) 10.
[8] S. Wen, Y. Li, N. Zheng, I.O. Raji, C. Yang, X. Bao, J. Mater. Chem. A 8 (2020) 13671.
[9] J. Yu, J.L. Ornelas, Y. Tang, M.A. Uddin, H. Guo, S. Yu, Y. Wang, H.Y. Woo, S. Zhang, G. Xing, X. Guo, W. Huang, ACS Appl. Mater. Interfaces 9 (2017) 42167.
[10] Y. Cui, H. Yao, J. Zhang, K. Xian, T. Zhang, L. Hong, Y. Wang, Y. Xu, K. Ma, C. An, C. He, Z. Wei, F. Gao, J. Hou, Adv. Mater. 32 (2020) 1908205.
[11] J. Hou, O. Inganas, R.H. Friend, F. Gao, Nat. Mater. 17 (2018) 119.
[12] D. Hu, Q. Yang, Y. Zheng, H. Tang, S. Chung, R. Singh, J. Lv, J. Fu, Z. Kan, B. Qin, Q. Chen, Z. Liao, H. Chen, Z. Xiao, K. Sun, S. Lu, Adv. Sci. 8 (2021) 2004262.
[13] F.C. Krebs, Sol. Energy Mater. Sol. Cells 93 (2009) 394.
[14] Y.W. Han, S.J. Jeon, H.S. Lee, H. Park, K.S. Kim, H. Lee, D.K. Moon, Adv. Energy Mater. 9 (2019) 1902065.
[15] S. Li, L. Ye, W. Zhao, H. Yan, B. Yang, D. Liu, W. Li, H. Ade, J. Hou, J. Am. Chem. Soc. 140 (2018) 7159.
[16] D. Gedefaw, A. Sharma, X. Pan, J.M. Bjuggren, R. Kroon, V.G. Gregoriou, C.L. Chochos, M.R. Andersson, Eur. Polym. J. 91 (2017) 92.
[17] S. Govaerts, J. Kesters, M. Defour, B. Van Mele, H. Penxten, S. Neupane, F.U. Renner, L. Lutsen, D. Vanderzande, W. Maes, Eur. Polym. J. 97 (2017) 49.
[18] D.H. Kim, Y.W. Han, D.K. Moon, Polymer (Guildf). 185 (2019).
[19] J. Yuan, Y. Zhang, L. Zhou, G. Zhang, H.L. Yip, T.K. Lau, X. Lu, C. Zhu, H. Peng, P.A. Johnson, M. Leclerc, Y. Cao, J. Ulanski, Y. Li, Y. Zou, Joule 3 (2019) 1140.
[20] Z. Wang, Z. Peng, Z. Xiao, D. Seyitliyev, K. Gundogdu, L. Ding, H. Ade, Adv. Mater. 32 (2020) 2005386.
[21] A. Armin, W. Li, O.J. Sandberg, Z. Xiao, L. Ding, J. Nelson, D. Neher, K. Vandewal, S. Shoaee, T. Wang, H. Ade, T. Heumüller, C. Brabec, P. Meredith, Adv. Energy Mater. 11 (2021) 2003570.
[22] Z. Luo, T. Liu, R. Ma, Y. Xiao, L. Zhan, G. Zhang, H. Sun, F. Ni, G. Chai, J. Wang, C. Zhong, Y. Zou, X. Guo, X. Lu, H. Chen, H. Yan, C. Yang, Adv. Mater. 32 (2020) 2005942.
[23] Z. Luo, R. Ma, T. Liu, J. Yu, Y. Xiao, R. Sun, G. Xie, J. Yuan, Y. Chen, K. Chen, G. Chai, H. Sun, J. Min, J. Zhang, Y. Zou, C. Yang, X. Lu, F. Gao, H. Yan, Joule 4 (2020) 1236.
[24] Z. Luo, R. Ma, Z. Chen, Y. Xiao, G. Zhang, T. Liu, R. Sun, Q. Zhan, Y. Zou, C. Zhong, Y. Chen, H. Sun, G. Chai, K. Chen, X. Guo, J. Min, X. Lu, C. Yang, H. Yan, Adv. Energy Mater. 10 (2020) 2002649.
[25] Z. Luo, T. Liu, H. Yan, Y. Zou, C. Yang, Adv. Funct. Mater. 30 (2020) 2004477.
[26] X. Guo, Q. Fan, J. Wu, G. Li, Z. Peng, W. Su, J. Lin, L. Hou, Y. Qin, H. Ade, L. Ye, M. Zhang, Y. Li, Angew. Chem. Int. Ed. 60 (2021) 2322.
[27] M. Zhang, L. Zhu, G. Zhou, T. Hao, C. Qiu, Z. Zhao, Q. Hu, B.W. Larson, H. Zhu, Z. Ma, Z. Tang, W. Feng, Y. Zhang, T.P. Russell, F. Liu, Nat. Commun. 12 (2021) 309.
[28] Q. Liu, Y. Jiang, K. Jin, J. Qin, J. Xu, W. Li, J. Xiong, J. Liu, Z. Xiao, K. Sun, S. Yang, X. Zhang, L. Ding, Sci. Bull. 65 (2020) 272.
[29] A.V. Akkuratov, I.E. Kuznetsov, P.M. Kuznetsov, N.V. Tukachev, I.V. Martynov, S. L. Nikitenko, A.V. Novikov, A.V. Chernyak, A. Zhugayevych, P.A. Troshin, Synth. Met. 259 (2020).
[30] M.H. Choi, H.Y. Kim, E.J. Lee, D. Kyung Moon, Polymer (Guildf). 91 (2016) 162.
[31] D.H. Kim, H.J. Song, S.W. Heo, K.W. Song, D.K. Moon, Sol. Energy Mater. Sol. Cells 120 (2014) 94.
[32] M. Schwarze, W. Tress, B. Beyer, F. Gao, R. Scholz, C. Poelking, K. Ortstein, A.A. Gunther, D. Kasemann, D. Andrienko, K. Leo, Science (80-.). 352 (2016) 1446.
[33] C. Poelking, M. Tietze, C. Elschner, S. Olthof, D. Hertel, B. Baumeier, F. Würthner, K. Meerholz, K. Leo, D. Andrienko, Nat. Mater. 14 (2014) 434.
[34] S. Li, B. Zhao, Z. He, S. Chen, J. Yu, A. Zhong, R. Tang, H. Wu, Q. Li, J. Qin, Z. Li, J. Mater. Chem. A 1 (2013) 4508.
[35] X. Pan, W. Xiong, T. Liu, X. Sun, L. Huo, D. Wei, M. Yu, M. Han, Y. Sun, 5 (2017) 4471.
[36] G. Zuo, Z. Li, M. Zhang, X. Guo, Y. Wu, S. Zhang, B. Peng, W. Wei, J. Hou, Polym. Chem. 5 (2014) 1976.
[37] X. Wang, Y. Sun, S. Chen, X. Guo, M. Zhang, X. Li, Y. Li, H. Wang, Macromolecules 45 (2012) 1208.
[38] H.J. Song, D.H. Kim, E.J. Lee, J.R. Haw, D.K. Moon, Sol. Energy Mater. Sol. Cells 123 (2014) 112.
[39] W. Chen, K. Tian, X. Song, Z. Zhang, K. Ye, G. Yu, Y. Wang, Org. Lett. 17 (2015) 6146.
[40] M. Irimia-Vladu, Y. Kanbur, F. Camaioni, M.E. Coppola, C. Yumusak, C.V. Irimia, A. Vlad, A. Operamolla, G.M. Farinola, G.P. Suranna, N. González-Benitez, M.C. Molina, L.F. Bautista, H. Langhals, B. Stadlober, E.D. Głowacki, N.S. Sariciftci, Chem. Mater. 31 (2019) 6315.
[41] H.A. Sung, D.H. Kim, T.H. Lee, M.H. Choi, E.J. Lee, D.K. Moon, J. Ind. Eng. Chem. 46 (2017) 304.
[42] H.J. Song, D.H. Kim, E.J. Lee, D.K. Moon, J. Mater. Chem. A 1 (2013) 6010.
[43] T.H. Lee, M.H. Choi, S.J. Jeon, D.K. Moon, Polymer (Guildf). 99 (2016) 756.
[44] H.J. Song, D.H. Kim, M.H. Choi, S.W. Heo, J.Y. Lee, J.Y. Lee, D.K. Moon, Sol. Energy Mater. Sol. Cells 117 (2013) 285.
[45] W. Lee, G.H. Kim, S.J. Ko, S. Yum, S. Hwang, S. Cho, Y.H. Shin, J.Y. Kim, H.Y. Woo, Macromolecules 47 (2014) 1604.
[46] S. Hedström, P. Persson, J. Phys. Chem. C 116 (2012) 26700.
[47] G. Lu, H. Usta, C. Risko, L. Wang, A. Facchetti, M.A. Ratner, T.J. Marks, J. Am. Chem. Soc. 130 (2008) 7670.
[48] C. Piliego, T.W. Holcombe, J.D. Douglas, C.H. Woo, P.M. Beaujuge, J.M.J. Fréchet, J. Am. Chem. Soc. 132 (2010) 7595.
[49] J. Rivnay, M.F. Toney, Y. Zheng, I.V. Kauvar, Z. Chen, V. Wagner, A. Facchetti, A. Salleo, Adv. Mater. 22 (2010) 4359.
[50] Q. Yang, C. Yan, J. Wu, X. Zhang, Y. Fu, Z. Xie, Org. Electron. 33 (2016) 55.
[51] J.Y. Lee, S.H. Kim, I.S. Song, D.K. Moon, J. Mater. Chem. 21 (2011) 16480.
[52] F. Liu, Y. Gu, C. Wang, W. Zhao, D. Chen, A.L. Briseno, T.P. Russell, Adv. Mater. 24 (2012) 3947.
[53] Y. Zhou, T.M. Khan, J.W. Shim, A. Dindar, C. Fuentes-Hernandez, B. Kippelen, J. Mater. Chem. A 2 (2014) 3492.
[54] Y. Cui, H. Yao, L. Hong, T. Zhang, Y. Tang, B. Lin, K. Xian, B. Gao, C. An, P. Bi, W. Ma, J. Hou, Natl. Sci. Rev. 7 (2020) 1239.
[55] R.J. Kline, M.D. McGehee, E.N. Kadnikova, J. Liu, J.M.J. Fréchet, M.F. Toney, Macromolecules 38 (2005) 3312.
[56] Z. Liang, M. Li, Q. Wang, Y. Qin, S.J. Stuard, Z. Peng, Y. Deng, H. Ade, L. Ye, Y. Geng, Joule 4 (2020) 1278.
[57] J. Xiao, X. Jia, C. Duan, F. Huang, H. Yip, Y. Cao, Adv. Mater. 2008158 (2021) 2008158.
[58] Y. Liu, K. Xian, Z. Peng, M. Gao, Y. Shi, Y. Deng, Y. Geng, L. Ye, J. Mater. Chem. A (2021), https://doi.org/10.1039/D1TA02253A.
[59] S.R. Cowan, N. Banerji, W.L. Leong, A.J. Heeger, Adv. Funct. Mater. 22 (2012) 1116.
[60] L.J.A. Koster, V.D. Mihailetchi, H. Xie, P.W.M. Blom, Appl. Phys. Lett. 87 (2005).
[61] C.M. Proctor, T.-Q. Nguyen, Appl. Phys. Lett. 106 (2015).
[62] J. Vollbrecht, V.V. Brus, S. Ko, J. Lee, A. Karki, D.X. Cao, K. Cho, G.C. Bazan, T. Nguyen, Adv. Energy Mater. 9 (2019) 1901438.